Tuijin Jishu/Journal of Propulsion Technology
ISSN: 1001-4055
Vol. 46 No. 2 (2025)

Influence of β-Al5FeSi Intermetallic Area Fraction on the Corrosion Rate of Horizontally Solidified Al-Si-Mg-Fe Alloys

Angela de Jesus Vasconcelos [1], Luane Luiza Pereira Marques [2], Héricles Ruiliman Oliveira de Souza [3], Leonardo Carvalho de Oliveira [4], Maria Adrina Paixão de Souza da Silva [5], Otávio Fernandes Lima da Rocha [6]

[1, 2, 3 ,4, 5, 6] *Federal University of Pará, UFPA, Brazil*

Abstract:- In this study, the corrosion behavior of an Al-7%Si-0.4%Mg-1.2%Fe alloy, obtained through horizontal solidification in a water-cooled device, was evaluated using the mass loss coupon test. The solidification process enabled the characterization of thermal parameters, including growth velocity (V_L) and cooling rate (T_R), which influence the formation of the β-Al5FeSi intermetallic phase and secondary dendritic spacing (λ_2). Samples with varying β-Al_5FeSi fractions were immersed in sulfuric acid solution, and corrosion rates were determined through mass loss measurements. The results revealed that increased fractions of β-Al_5FeSi correlate with higher corrosion rates, highlighting the detrimental effect of this intermetallic phase on the alloy's corrosion resistance. These findings emphasize the critical role of cooling rates and microstructural refinement in reducing the presence of β-Al_5FeSi and improving the alloy's performance in corrosive environments.

Keywords: *Al-Si-Fe Alloys, Mass Loss Test, Cooling.*

1. Introduction

The modern world increasingly demands lightweight structural materials to improve fuel economy, reduce energy consumption, and lower greenhouse gas emissions in industrial sectors. Aluminum alloys, due to their low density, high stiffness-to-weight ratio, good formability, and excellent corrosion resistance, have become essential in the manufacture of components for automotive, aerospace, and naval applications [1].

Despite their advantageous properties, aluminum alloys are still susceptible to corrosion, particularly in aggressive environments. Corrosion has been a recurring challenge in industries where these alloys are employed, such as aerospace, automotive, and marine sectors. Although aluminum naturally forms a protective oxide layer (Al_2O_3), this passive film may not be sufficient to prevent various forms of localized corrosion, including pitting, intergranular attack, galvanic corrosion, and stress corrosion cracking [2], [3].

Corrosion of metallic materials is an electrochemical phenomenon resulting from the interaction between chemical agents in the environment and the metal surface. When corrosion occurs in aqueous media, it typically involves redox reactions, where anodic regions undergo metal oxidation and cathodic regions promote reduction reactions—commonly the reduction of hydronium ions and release of hydrogen gas. This process may be intensified by factors such as temperature, humidity, mechanical stress, and the presence of aggressive ions [4], [5].

In aluminum-silicon (Al-Si) alloys, the presence of iron, whether as an impurity or alloying addition, leads to the formation of intermetallic phases, notably β-Al_5FeSi. This phase typically exhibits a platelet-like or needle-shaped morphology and is characterized by high brittleness, which negatively affects both mechanical strength and corrosion performance. Formed primarily along interdendritic regions, β-Al_5FeSi can act as cathodic sites in galvanic interactions with the aluminum matrix, accelerating localized corrosion, particularly in chloride-rich environments [6], [8].

The formation, size, and distribution of β-Al_5FeSi are highly sensitive to the solidification conditions. Slow cooling or diffusive regimes favor the growth of long, interconnected β-phase structures, whereas directional solidification under thermal gradients tends to refine and disperse these intermetallics, as shown on the thermal behavior and pseudo-binary diagram of the Al-7.0wt%Si-0.4wt%Mg-xwt%Fe alloy (Fig. 1 a and b, respectively) [8]. Previous studies [9], [10] show that corrosion often initiates at these intermetallic sites due to poor oxide film adhesion or microcracks caused by residual thermal stress. Modifying the alloy composition through the addition of Mn, Cr, or rare earth elements can suppress β-phase formation and promote the formation of more compact α-Al (Fe,Mn)Si phases, which are less harmful to corrosion resistance [7].

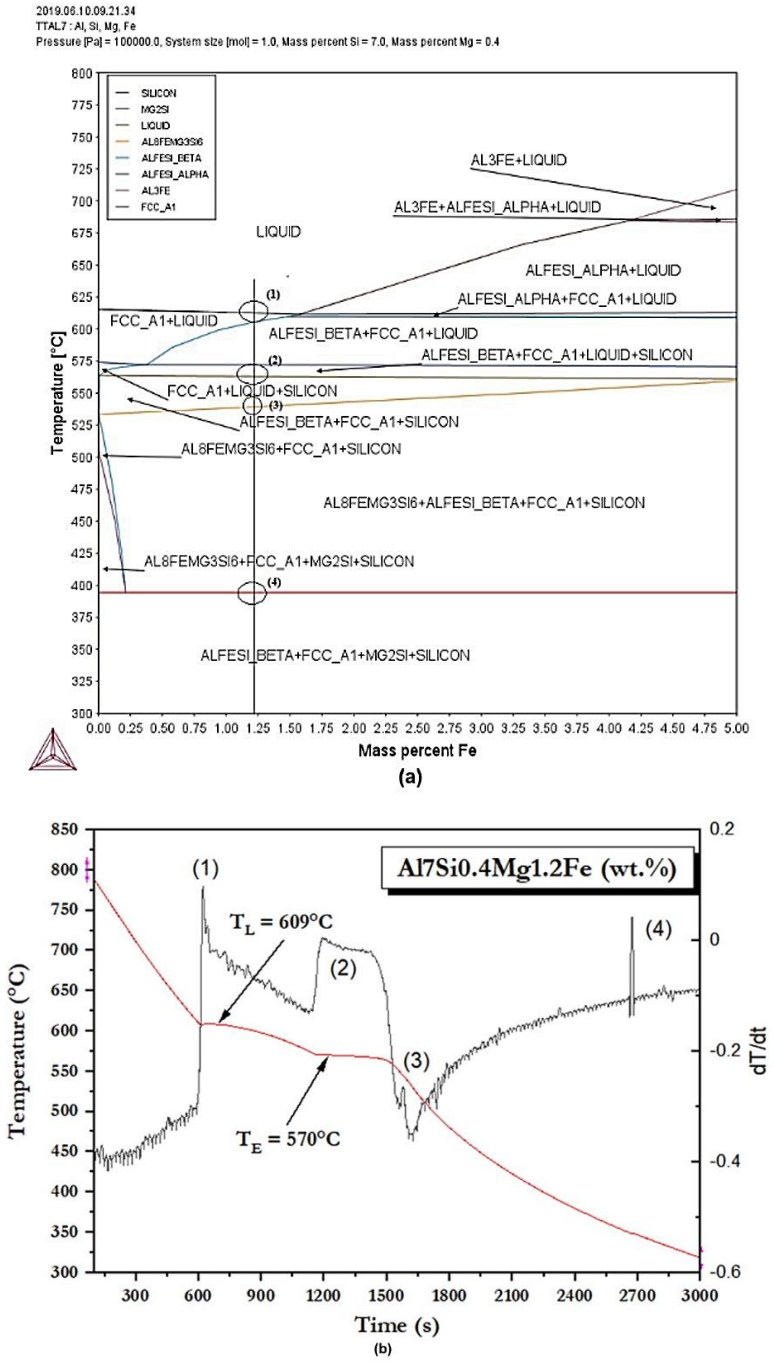

Fig. 1 - (a) Pseudo-binary phase diagram for the Al7Si0.4MgxFe alloy and (b) experimental cooling curve of the investigated alloy under slow cooling.

Vasconcelos *et al.,* 2021.

The Mn/Fe ratio is particularly critical, as it dictates the type and proportion of intermetallic compounds formed under different cooling conditions. Such alloy design considerations, combined with process control, are fundamental for optimizing corrosion performance [11].

To quantify corrosion behavior, gravimetric techniques such as the mass loss coupon test are widely adopted due to their simplicity, reproducibility, and direct correlation with material degradation [12]. These methods, when combined with microstructural characterization - such as phase morphology, size, and area fraction- enable a comprehensive evaluation of corrosion mechanisms in Al alloys.

In this context, the present study investigates the corrosion behavior of an Al-7%Si-0.4%Mg-1.2%Fe alloy subjected to immersion in sulfuric acid solution. This evaluation contributes to understanding the degradation mechanisms involved and to proposing strategies for improving the corrosion performance of iron-containing Al-Si alloys in industrial applications.

2. Methodology

An Al-7%Si-0.4%Mg-1.2%Fe alloy was produced via horizontal directional solidification in a water-cooled steel mold. Thermocouples were placed along the length of the ingot to monitor thermal gradients. Samples were cut from positions 5, 15, 20, 30, 50, and 90 mm from the chilled end to capture a range of cooling rates.

Each sample underwent standard metallographic preparation and was analyzed by optical microscopy and scanning electron microscopy (SEM) for microstructural evaluation. Image analysis was used to quantify the size and area fraction of β-Al_5FeSi. The length of the intermetallics was measured from high-resolution SEM images using linear interception techniques. The schematic representation of the process is shown in Fig. 2, but the detailed methodology can be found in Vasconcelos *et al*. [8].

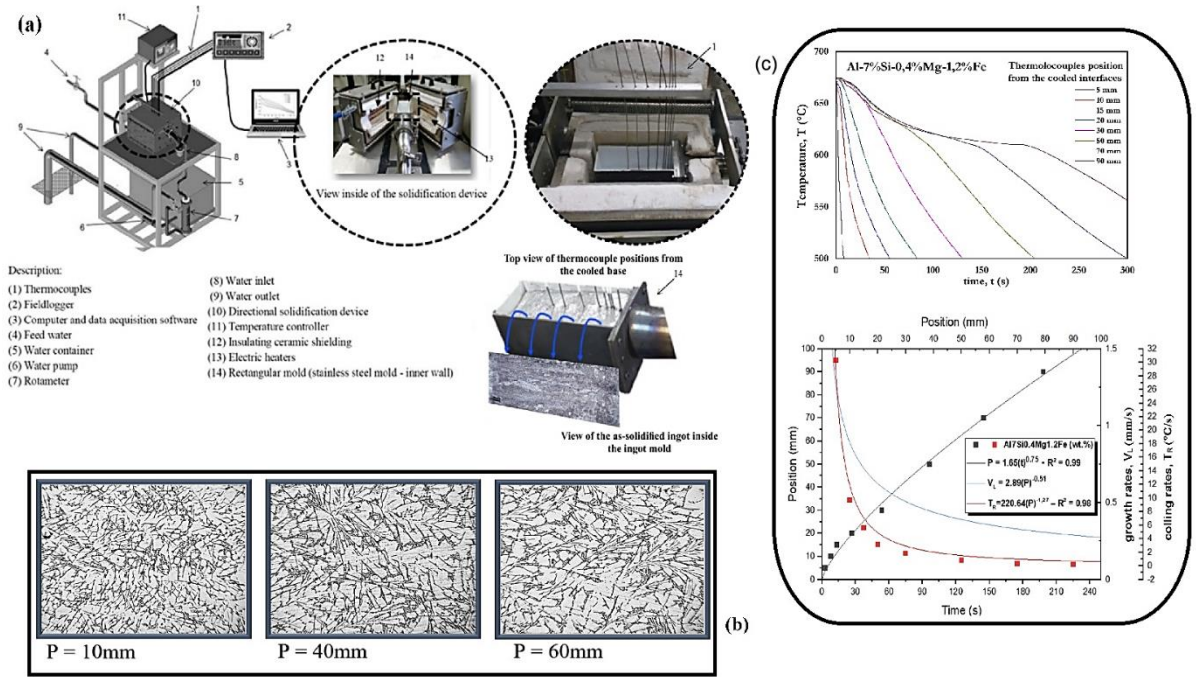

Fig. 2 - Schematic representation of the solidification process, showing: (a) Complete scheme of the solidification furnace, with details of the horizontal water-cooled device, detailed positioning of the thermocouples in the ingot and as-cast ingot of the investigated alloy, showing the longitudinal section for microstructural analysis, (b) Typical solidification structures for the Al7Si0.4Mg1.2Fe alloy (wt.%), resulting from the unsteady-state horizontal solidification process and (c) Thermal analysis resulting from the transient horizontal solidification of the investigated alloy.

Adapted from Vasconcelos *et al*. [8].

Corrosion resistance was quantitatively evaluated using the mass loss coupon method, following procedures adapted from ASTM G31 [13]. Rectangular prism-shaped specimens were extracted from different positions (5, 15, 20, 30, 50, and 90 mm) along the directionally solidified Al-7%Si-0.4%Mg-1.2%Fe (wt%) ingot.

Each specimen was polished using successive SiC sandpapers up to 1200 grit, followed by thorough cleaning in deionized water and ethanol. The initial mass (W_0) of each sample was measured using an analytical balance with ±0.1 mg resolution. All coupons were immersed in 100 mL of 10N H_2SO_4 solution for 168 hours (7 days) at room temperature (~25 °C), without stirring.

After the exposure period, the samples were rinsed in deionized water, then in ethanol, and finally dried in warm air. Corrosion products were removed using a soft brush and, when necessary, immersion in a neutral cleaning solution to ensure only base metal loss was accounted. The final mass (Wf) was then recorded. The corrosion rate (CR) was calculated in millimeters per year (mm/year) using the standard gravimetric formula (1):

$$CR = (87.6 \times (W_0 - Wf)) / (\rho \times A \times t) \quad (1)$$

Where:

- $(W_0 - Wf)$ = mass loss (mg);
- ρ = alloy density (assumed as 2.69 g/cm³);
- A = exposed surface area of the coupon (cm²);
- t = immersion time (hours);
- 87.6 = unit conversion constant.

Each position was evaluated in triplicate to ensure reproducibility, and the mean corrosion rate was used for analysis. The immersion setup was schematically represented in Figs. 3 and 4. Visual inspection of the samples after corrosion was carried out under a stereomicroscope to identify surface degradation modes, as illustrated in Fig. 5.

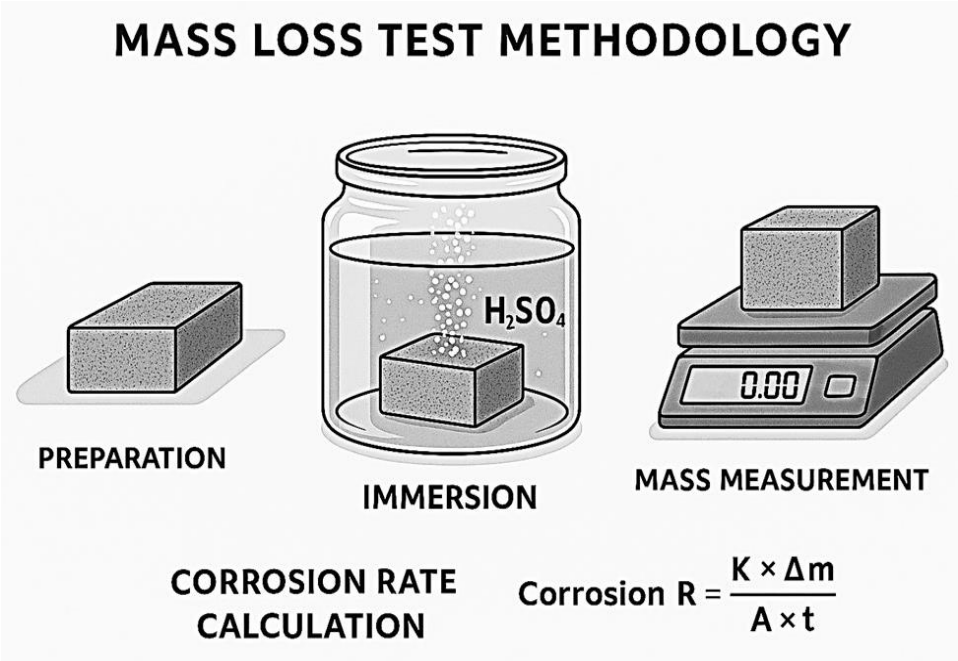

Fig. 3 - Schematic representation of the procedure. It involves surface preparation, immersion in H_2SO_4 for a fixed exposure time, mass measurement, and corrosion rate calculation using the standard gravimetric equation.

AI-generated illustration

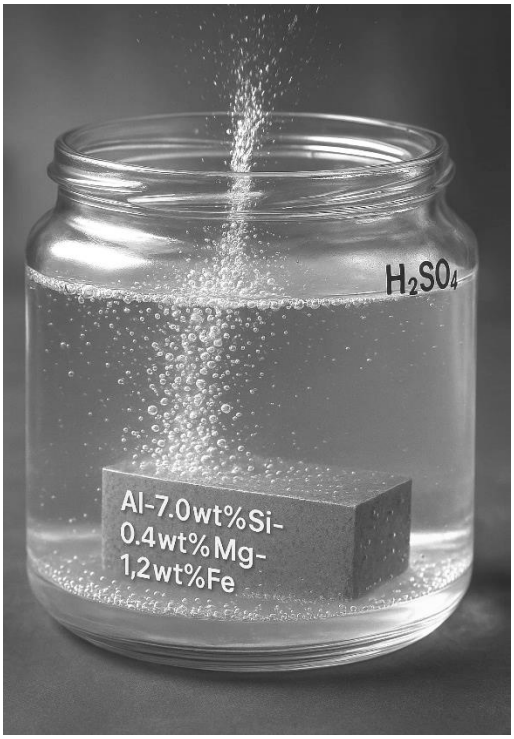

Fig. 4 - Schematic representation of the immersion corrosion test. A prism-shaped specimen of Al–7.0 wt% Si–0.4 wt% Mg–1.2 wt% Fe alloy is immersed in 10N H_2SO_4 solution. The formation of hydrogen bubbles on the surface indicates active metal dissolution, used to evaluate corrosion behavior by mass loss analysis.

AI-generated illustration

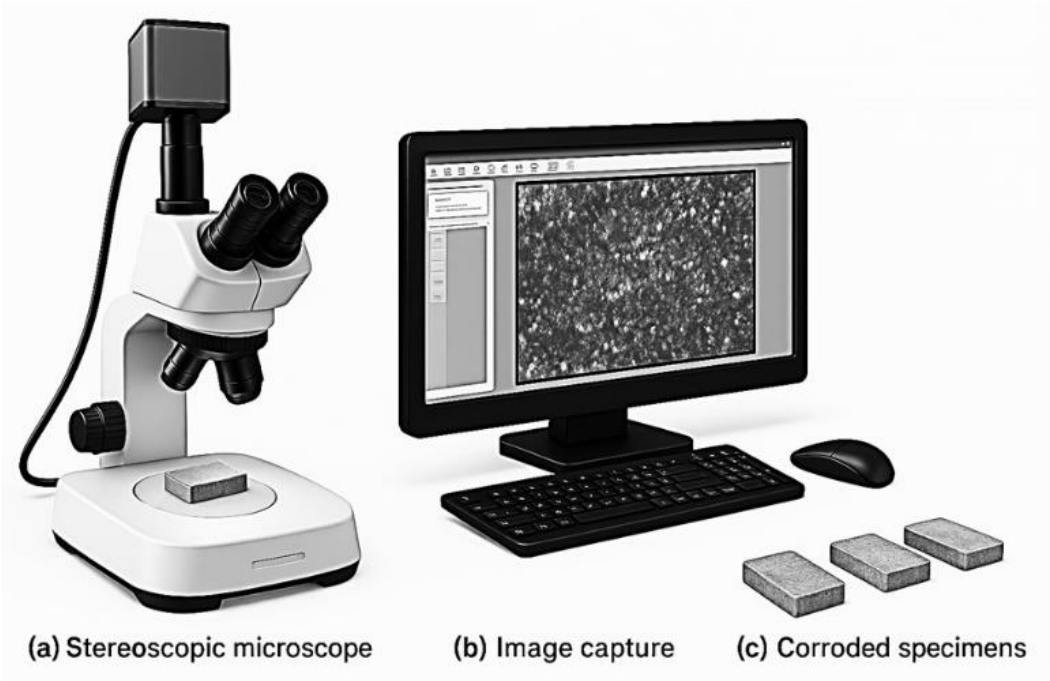

Fig. 5 - Visual inspection of the samples, showing (a) Stereomicroscope, (b) image capture and (c) corroded specimens.

AI-generated illustration

3. Results and Discussion

The corrosion rate exhibited a distinct and non-linear progression along the length of the directionally solidified ingot, reflecting the microstructural evolution imposed by the thermal gradient during solidification, as presented in Fig. 6.

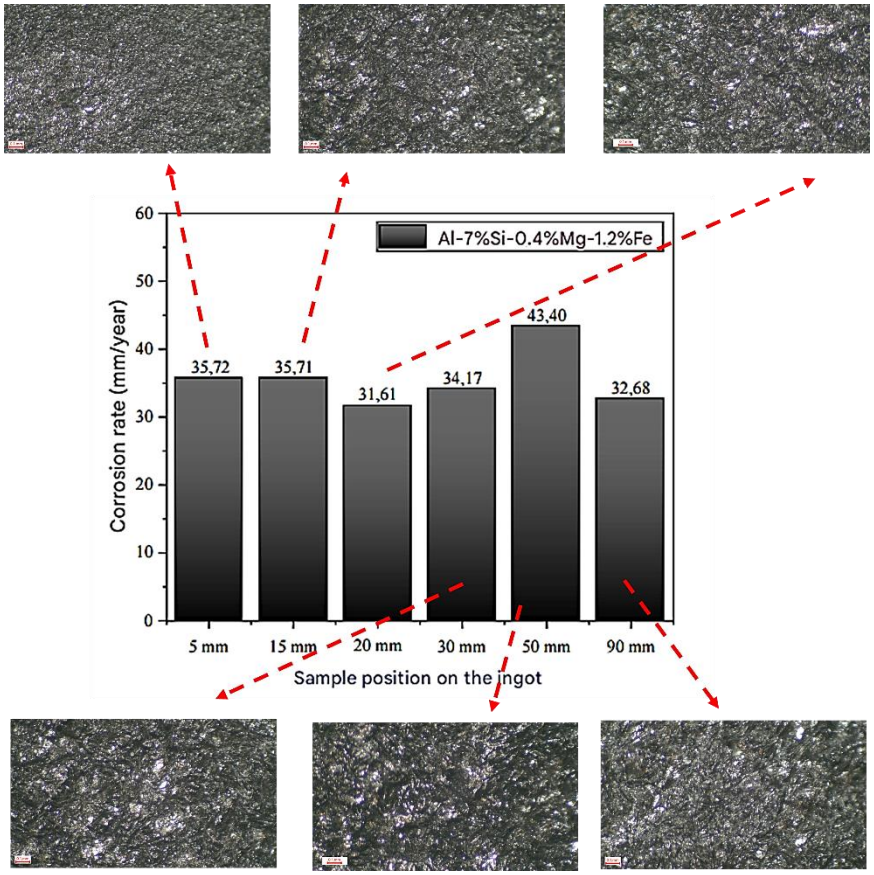

Fig. 6 - Corrosion rates obtained by mass loss coupon testing for samples of Al–7.0 wt% Si–0.4 wt% Mg–1.2 wt% Fe alloy extracted at different positions along the solidified ingot. The central bar chart shows the average corrosion rate (mm/year) for each position, while the surrounding stereomicroscope images illustrate the corroded surfaces.

By Author

At 5 mm and 15 mm, which correspond to regions closer to the chilled mold wall, the cooling rate was highest, leading to finer secondary dendritic arm spacings (λ_2) and rapid solidification kinetics, as found on results from Vasconcelos et al. [8], Fig. 7. Under these conditions, the β-Al5FeSi phase nucleated as short, discontinuous needles or platelets, with lower area fractions and minimal interconnectivity, as shown in Fig. 8. The refinement and dispersion of β intermetallics in these regions likely contributed to the uniform corrosion behavior observed, as the passive aluminum oxide film remained stable across the surface. The corrosion rates in these zones, approximately 35.7 mm/year, were the lowest recorded in the ingot. This behavior is consistent with the literature, where finely dispersed β-Al_5FeSi has reduced cathodic influence, minimizing galvanic coupling with the α-Al matrix [8], [14], [15].

At 30 mm and especially 50 mm, the microstructure exhibited a transition to coarser, elongated, and partially interconnected β-Al_5FeSi particles. This change is attributed to lower local cooling rates and extended solidification times, promoting directional growth of the intermetallic phase along interdendritic paths. These morphologies significantly increased the local cathodic surface area, destabilizing the passive film and facilitating microgalvanic cell formation. SEM images revealed clustered platelets forming networks that intersected the

aluminum matrix (Figs. 7 (c) and 8 (b)). These structural features acted as initiation sites for pitting corrosion, allowing for deeper penetration of the electrolyte and increased loss of metal through localized attacks.

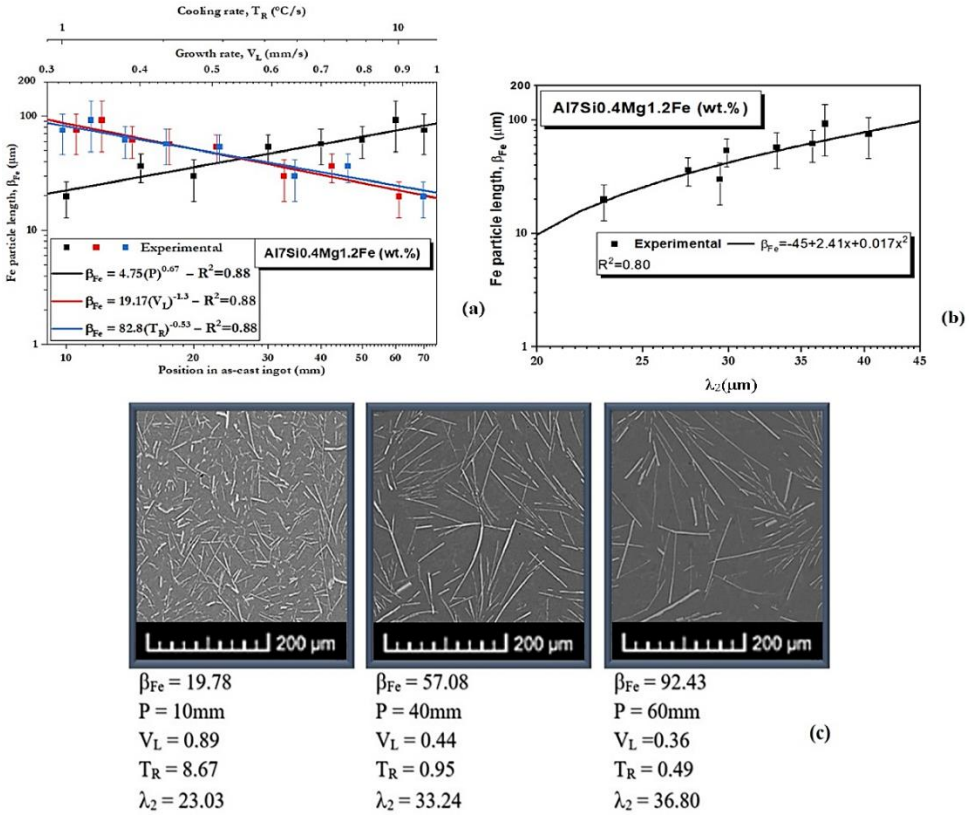

Fig. 7 - (a) and (b) Fe particle length (βFe) dependence as a function of the position in the as-cast ingot and thermal parameters (V_L and T_R), respectively, and (c) SEM micrographs, showing the βFe variation.

Vasconcelos *et al.,* 2021.

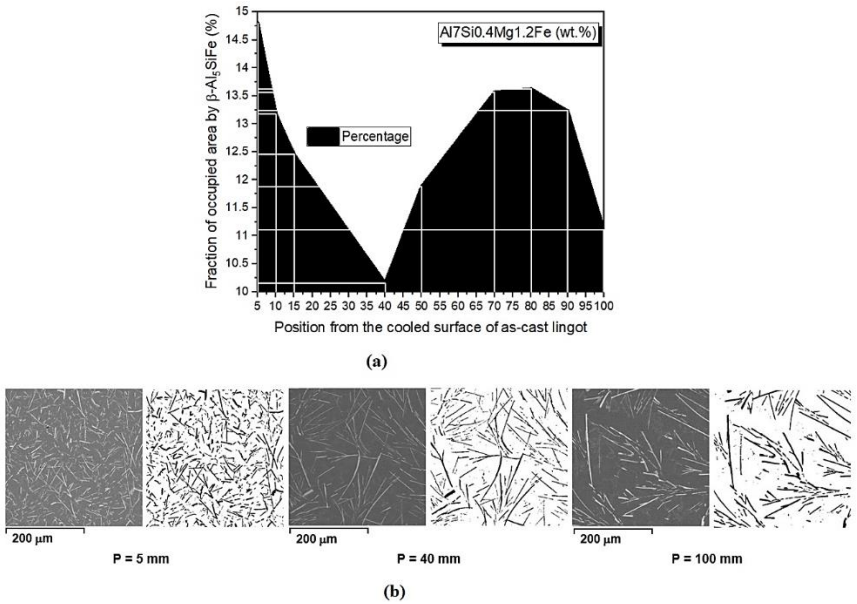

Fig. 8 - (a) Area fraction of occupied area by needle-like β-Al_5FeSi particle in as-cast samples from the cooled base and (b) original and binarized SEM microstructures for three positions form the cooled base.

Vasconcelos *et al*., 2021.

As a result, the corrosion rate peaked at 50 mm (43.4 mm/year), coinciding with the highest measured β-phase area fraction and particle length. This peak reinforces the direct link between β-phase morphology and corrosion behavior. The results presented confirm the inference of the findings reported by Vasconcelos *et al*. [8], who observed that the coarsening and clustering of β-Al_5FeSi leads to mechanical weakness and electrochemical vulnerability. Diler *et al*. [16] also reported increased current densities in aluminum alloys with coarse intermetallics, correlating with greater mass loss in gravimetric tests.

At 90 mm, further from the mold interface, the corrosion rate decreased to 32.68 mm/year. While the β-Al5FeSi phase remained coarse due to slower cooling, its spatial distribution appeared less connected. This decrease in connectivity has likely diminished galvanic interactions between cathodic intermetallics and the anodic aluminum matrix, reducing localized electrochemical gradients and stabilizing the oxide layer. Moreover, the potential for pit coalescence was lower, contributing to more homogeneous surface degradation.

These findings are consistent with both the literature review by Berlanga-Labari *et al*. [14] and the experimental results presented by Qi *et al.* [15]. Berlanga-Labari et al. emphasized the detrimental role of Fe-rich intermetallics, particularly β-Al_5FeSi, in cast aluminum alloys. Their presence - especially when coarse or interconnected - promotes localized corrosion through the formation of microgalvanic cells with the aluminum matrix. This aligns with the corrosion rate evolution observed in the present study, which peaked at 50 mm, precisely where β-phase particles were longest and most interconnected due to lower local cooling rates. Their review also reinforces the importance of intermetallic morphology, spatial distribution, and solidification control in mitigating corrosion, supporting the structure-property correlations identified herein.

Complementarily, Qi et al. demonstrated that the refinement and reduced connectivity of β-Al_5FeSi intermetallics - achieved via Rheo-HPDC processing - significantly improved corrosion resistance in Al-Si-Fe alloys. Both their study and the present work confirm that coarse, elongated β-phase particles increase galvanic coupling with the matrix, promoting pitting and mass loss. Although Qi et al. employed electrochemical and SKP techniques in NaCl solution, and the current study used gravimetric evaluation in sulfuric acid, the correlation between intermetallic architecture and corrosion susceptibility was consistently observed across both methodologies.

Overall, the results support the hypothesis that not only the presence but also the size, morphology, and spatial continuity of β-Al5FeSi play critical roles in governing corrosion behavior. High aspect-ratio platelets and their alignment along solidification fronts enhance their galvanic effect, especially when clustered. Conversely, reduced connectivity and refined morphology tend to improve corrosion resistance, even in regions where particle size remains elevated.

4. Conclusion

This study highlights the critical influence of β-Al_5FeSi intermetallic characteristics—particularly size, morphology, and spatial distribution—on the corrosion performance of Al-7%Si-0.4%Mg-1.2%Fe (wt%) alloys directionally solidified under a horizontal thermal gradient. The findings reinforce the notion that corrosion in Al-Si-Fe systems is not solely governed by the presence of Fe-rich phases, but by their geometric and distributional attributes within the microstructure.

The observed non-linear trend in corrosion rate, peaking at intermediate ingot positions (notably 50 mm), underscores the need to precisely control solidification parameters to avoid morphologies prone to microgalvanic effects. In particular, the alignment and clustering of elongated β-phase platelets serve as critical pathways for localized attack, validating concerns previously raised in the literature.

From a practical standpoint, this work contributes to the understanding of how solidification design - alongside alloy chemistry - can be employed as a strategic tool to mitigate corrosion in cast Al alloys. These insights can be applied to industries requiring high corrosion resistance, such as marine, transport, and structural applications, especially when using recycled alloys with elevated Fe contents.

Future research could explore alloy modifications using Mn or rare earth elements to promote benign intermetallics and extend the methodology to assess corrosion behavior under simulated service conditions.

Furthermore, integrating electrochemical impedance spectroscopy and 3D tomography could enhance the predictive modeling of corrosion based on intermetallic architecture.

Acknowledgement:

The authors gratefully acknowledge the Federal University of Pará (UFPA) for providing the infrastructure and research facilities essential to this work. Financial support from the Coordination for the Improvement of Higher Education Personnel (CAPES – Finance Code 001) and the National Council for Scientific and Technological Development (CNPq – Brazil) is also acknowledged.

References

[1] J. Hirsch and T. Al-Samman, "Superior light metals by texture engineering: Optimized aluminum and magnesium alloys for automotive applications," *Acta Materialia*, vol. 61, no. 3, pp. 818–843, Feb. 2013, doi: https://doi.org/10.1016/j.actamat.2012.10.044

[2] Y. Liu *et al.*, "Experimental and theoretical study on corrosion mechanism of aluminium alloy in different corrosive solutions," *Journal of Molecular Liquids*, vol. 412, pp. 125894–125894, Aug. 2024, doi: https://doi.org/10.1016/j.molliq.2024.125894

[3] H. Zhu, M. Leng, G. Jin, and H. Miao, "A Review of Research on Galvanic Corrosion of Aluminum Alloys," *Fluid dynamics & materials processing*, vol. 19, no. 7, pp. 1907–1923, Jan. 2023, doi: https://doi.org/10.32604/fdmp.2023.025416

[4] G. Zhou, K. A. Unocic, C. Wang, Z. Shan, S. J. Haigh, and J. C. Yang, "Revealing atomic-to-nanoscale oxidation mechanisms of metallic materials," *MRS Bulletin*, vol. 48, no. 8, pp. 852–863, Aug. 2023, doi: https://doi.org/10.1557/s43577-023-00595-4.

[5] D.-H. Xia, C.-M. Deng, D. Macdonald, S. Jamali, D. Mills, J.-L. Luo, M. G. Strelb, M. Amiri, W. Jin, S. Song, and W. Hu, "Electrochemical measurements used for assessment of corrosion and protection of metallic materials in the field: A critical review," *Journal of Materials Science & Technology*, vol. 112, pp. 151–183, Jun. 2022, doi: https://doi.org/10.1016/j.jmst.2021.11.004.

[6] M. Qi, Y. Kang, Q. Qiu, W. Tang, J. Li, and B. Li, "Microstructures, mechanical properties, and corrosion behavior of novel high-thermal-conductivity hypoeutectic Al-Si alloys prepared by rheological high pressure die-casting and high pressure die-casting," *Journal of Alloys and Compounds*, vol. 749, pp. 487–502, Jun. 2018, doi: https://doi.org/10.1016/j.jallcom.2018.03.178

[7] Z. Wang, T. Ma, W. Han, and G. Yu, "Corrosion behavior on aluminum alloy LY12 in simulated atmospheric corrosion process," *Transactions of Nonferrous Metals Society of China*, vol. 17, no. 2, pp. 326–334, Apr. 2007, doi: https://doi.org/10.1016/s1003-6326(07)60093-4.

[8] Vasconcelos, H. Azevedo, A. Barros, O. Rocha, and M. M. Melo, "Influence of the dendritic microstructure and β-Al5FeSi phase on the wear characteristics in a horizontally solidified Al-7Si-0.4Mg-1.2Fe alloy," *Materials Today Communications*, vol. 26, p. 102099, Mar. 2021, doi: https://doi.org/10.1016/j.mtcomm.2021.102099

[9] L. Kuchariková, E. Tillová, J. Belan, M. Chalupová, I. Švecová, R. Čička[2], and M. Uhríčik, "Observation on the Formation of β-Al5FeSi Phase Depending on the Content of Fe in Aluminium Cast Alloy," *Manufacturing Technology*, vol. 18, no. 4, pp. 611–615, Sep. 2018, doi: https://doi.org/10.21062/ujep/147.2018/a/1213-2489/mt/18/4/611

[10] D. Medvecká, L. Kuchariková, and M. Uhríčik, "The Failure Degradation of Recycled Aluminium Alloys with High Content of β-Al_5FeSi Intermetallic Phases," *Defect and diffusion forum/Diffusion and defect data, solid state data. Part A, Defect and diffusion forum*, vol. 403, pp. 97–102, Sep. 2020, doi: https://doi.org/10.4028/www.scientific.net/ddf.403.97

[11] Z. Xu, X. Zhang, H. Wang, A. Gao, T. Ma, and H. Song, "Effect of Mn/Fe ratio on the microstructure and properties of 6061 sheets obtained by twin-roll cast," *Materials characterization*, vol. 168, pp. 110536, Oct. 2020, doi: https://doi.org/10.1016/j.matchar.2020.110536

[12] Y. Liang, Y. Du, Z. Zhu, L. Chen, Y. Liu, L. Zhang, and L. Qiao, "Investigation on AC corrosion of aluminum alloy sacrificial anode in the artificial simulated seawater environment," *Electrochimica Acta*, vol. 446, pp. 142002, Apr. 2023, doi: https://doi.org/10.1016/j.electacta.2023.142002

[13] *ASTM International, Standard Practice for Laboratory Immersion Corrosion Testing of Metals, ASTM G31-21, West Conshohocken, PA, USA, 2021.*

[14] C. Berlanga-Labari, M. V. Biezma-Moraleda, and P. J. Rivero, "Corrosion of Cast Aluminum Alloys: A Review," *Metals*, vol. 10, no. 10, p. 1384, Oct. 2020, doi: https://doi.org/10.3390/met10101384

[15] M. Qi, Y. Kang, J. Li, and B. Shang, "Improvement in mechanical, thermal conductivity and corrosion performances of a new high-thermally conductive Al-Si-Fe alloy through a novel R-HPDC process," *Journal of materials processing technology*, vol. 279, pp. 116586, May 2020, doi: https://doi.org/10.1016/j.jmatprotec.2019.116586

[16] E. Diler, F. Peltier, J. Becker, and D. Thierry, "Real-time corrosion monitoring of aluminium alloys under chloride-contaminated atmospheric conditions," *Materials and Corrosion*, vol. 72, pp. 1377-1387, Jan. 2021, doi: https://doi.org/10.1002/maco.202112302